NANO LETTERS

Letter

pubs.acs.org/NanoLett

Multifunctional Superhydrophobic Surfaces Templated From Innately Microstructured Hydrogel Matrix

Yaqun Wang,[†,∥] Ye Shi,[‡,§,∥] Lijia Pan,[*,†] Meng Yang,[†] Lele Peng,[‡,§] Shi Zong,[†] Yi Shi,[*,†] and Guihua Yu[*,‡,§]

[†]Collaborative Innovation Center of Advanced Microstructures, Jiangsu Provincial Key Laboratory of Photonic and Electronic Materials, School of Electronic Science and Engineering, Nanjing University, Nanjing 210093, China

[‡]Materials Science and Engineering Program and [§]Department of Mechanical Engineering, The University of Texas at Austin, Austin, Texas 78712, United States

S *Supporting Information*

ABSTRACT: Superhydrophobic surfaces are of immense scientific and technological interests for a broad range of applications. However, a major challenge remains in developing scalable methodologies that enable superhydrophobic coatings on versatile substrates with a combination of strong mechanical stability, optical transparency, and even stretchability. Herein, we developed a scalable methodology to versatile hydrophobic surfaces that combine with strong mechanical stability, optical transparency, and stretchability by using a self-assembled hydrogel as the template to in situ generate silica microstructures and subsequent silanization. The superhydrophobic coatings can be enabled on virtually any substrates via large-area deposition techniques like dip coating. Transparent surfaces with optical transmittance as high as 98% were obtained. Moreover, the coatings exhibit superior mechanical flexibility and robustness that it can sustain contact angles ~160° even after 5000 cycles of mechanically stretching at 100% strain. The multifunctional surfaces can be used as screen filters and sponges for the oil/water separation that can selectively absorb oils up to 40× their weight.

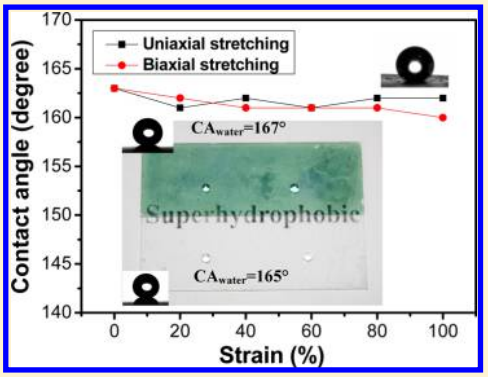

KEYWORDS: *Superhydrophobic surfaces, hydrogels, multifunctional, stretchable, transparent, hierarchical, coatings*

Robust superhydrophobic surfaces that stably trap micropockets of air beneath the water drop to maintain a Cassie state and exhibit macroscopic contact angles (CA) greater than 150° and roll-off/tilt angles (TA) below 10° have been of immense scientific and technological interests for a broad range of applications.[1−5] Introducing micro/nanostructures to obtain an appropriate surface roughness is the prerequisite for superhydrophobicity.[6] Synthetic surfaces have been recently developed based on low-energy surface and multiscale roughness by various micro/nanotechniques such as chemical vapor/bath deposition,[3,7−9] particle/nanowire assemblies,[4,10−12] polymer membrane casting,[13] and electrospinning.[14,15] A major challenge remains in developing scalable methodologies that enable superhydrophobic coatings on versatile substrates (regardless of composition, morphology/shape, and size) with a combination of strong mechanical and chemical stability, optical transparency, and even stretchability.

In this study, we present a new type of superhydrophobic surface in which the key layer composed of a three-dimensional (3D) silica nanostructure is in situ replicated from a hydrogel template. The resulting hybrid coatings have the morphology similar to that of the lower surface of the lotus leaf and exhibit excellent superhydrophobic properties after silanization. Because the hydrogel precursors have good wettability, our hydrogel nanostructure-based coatings are versatile and ready for coating onto virtually any substrates, including metals, cement, wood, fabrics, and plastics. Moreover, the superhydrophobic surfaces exhibit strong mechanical properties in that it is flexible, mechanically robust and can sustain superhydrophobicity under thousands cycles of extensive stretching. In addition, we demonstrate the applications of these versatile surfaces as selective filters and sponges for the oil/water separation, which can continuously separate oils with the residue water contents less than 0.04% and selectively absorb oils up to 40× their weight, respectively. Our results suggest this novel multifunctional superhydrophobic coating can be useful for flexible water-proof coatings, self-cleaning surfaces, antifouling surfaces, industry oil recovery and oil spill cleaning.

The superhydrophobic surfaces are obtained by in situ templating the nanostructures against the polyaniline (PAni) hydrogel, as schematically illustrated in Scheme 1. In the first step, the following precursor solutions were mixed: Solution A, aqueous solution of oxidative initiator; Solution B, aqueous solution of aniline monomer and phytic acid; and Solution C, teraethoxysilane (TEOS) in isopropanol. The polymerization

Received: May 27, 2014
Published: June 30, 2014

   dx.doi.org/10.1021/nl5019782 | *Nano Lett.* 2014, 14, 4803−4809

Scheme 1. Schematic Illustration of Superhydrophobic Surfaces Based on Hydrogel Template[a]

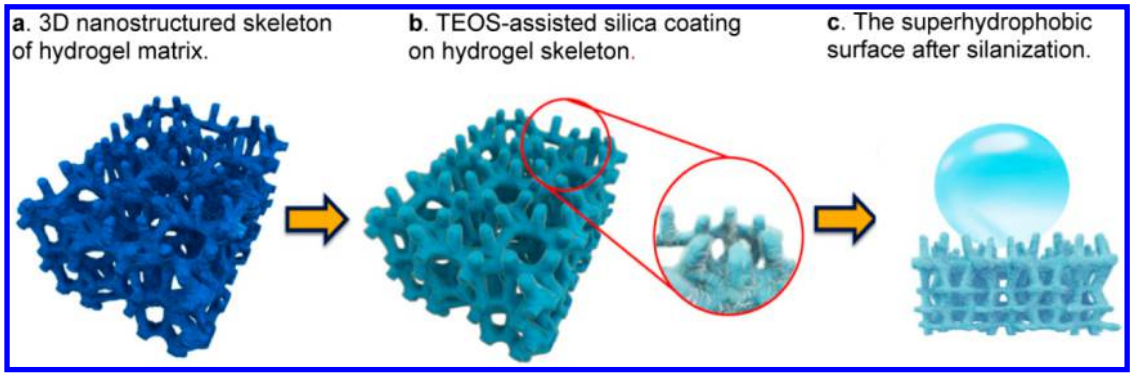

[a](a) The 3D nanostructured skeleton resulted from the rapid gelling of PAni hydrogel. (b) Uniform silica layer in situ formed on PAni hydrogel matrix via TEOS-based hydrolysis. (c) A water drop deposited on a superhydrophobic 3D nanostructured surface.

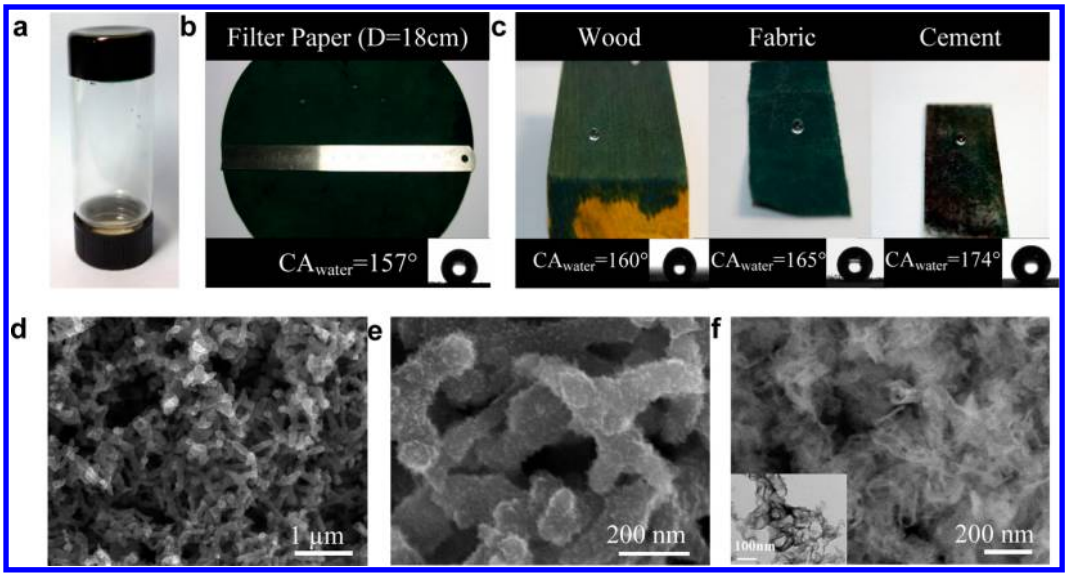

Figure 1. Digital photographs and SEM images of superhydrophobic surfaces. (a) Photograph of the silica/PAni hybrid hydrogel. (b,c) Photographs of the superhydrophobic coatings on filter paper, wood, fabric, and cement. (d,e) SEM images of the silica/PAni hybrid nanostructures. (f) SEM image of the silica microstructures after the PAni core was removed (inset, TEM image revealing its nanotube structure).

and gelling of PAni was relatively fast, forming into three-dimensional (3D) hierarchical structured hydrogel within 3 min (Scheme 1a and Figure 1a).[16] It is worth noting that the acidic high-water-content hydrogel matrix allowed for an in situ Stöber reaction of TEOS,[17] resulting in a silica layer preferentially coated on the PAni nanostructural template (Scheme 1b). In the second step, the silica layer was silanized by deposition of trichloro(octadecyl)silane (OTS) to produce a superhydrophobic surface (Scheme 1c). The hydrogel-templating method is versatile as we have fabricated stable, conformal superhydrophobic coatings on various substrates including paper, wood, cotton fabric, cement, glass, metal, plastic, and rubbers (Figure 1b,c and Table 1).

The morphologies and structures of the hydrogel based surfaces were characterized by scanning electron microscopy (SEM) and transmission electron microscopy (TEM). Figure 1d shows a typical SEM image of the coating, which consists of 3D interconnected nanofibers with uniform diameters of approximately 100 nm and is similar to the morphology of the lower surface of lotus leaves.[6] The magnified SEM image (Figure 1e) reveals the nanoscale roughness on the nanofiber surface. Such a nanoscale convex can provide an energy barrier against the wetting of nanofibers with interface pinning.[18] SEM image (Figure 1f) shows that only silica nanotube networks remained in the coating and the PAni core has been fully removed after the film was calcinated at 400 °C for 2 h. The

Table 1. Comparison of the Static Contact Angles (CAs) of Water on the Silica/PAni Hybrid Surfaces and the Pristine Substrates

substrates	static CA on initial substrates	static CA on silica/PAni surface
glass	46°	167°
aluminum foil	92°	157°
stainless steel screen	122°	149°
sponge	90°	164°
paper (A4)	69°	169°
filter paper	absorbed	157°
wood	26°	160°
cement	absorbed	174°
fabric	absorbed	165°
PDMS	119°	163°
PMMA	91°	161°

dx.doi.org/10.1021/nl5019782 | Nano Lett. 2014, 14, 4803−4809

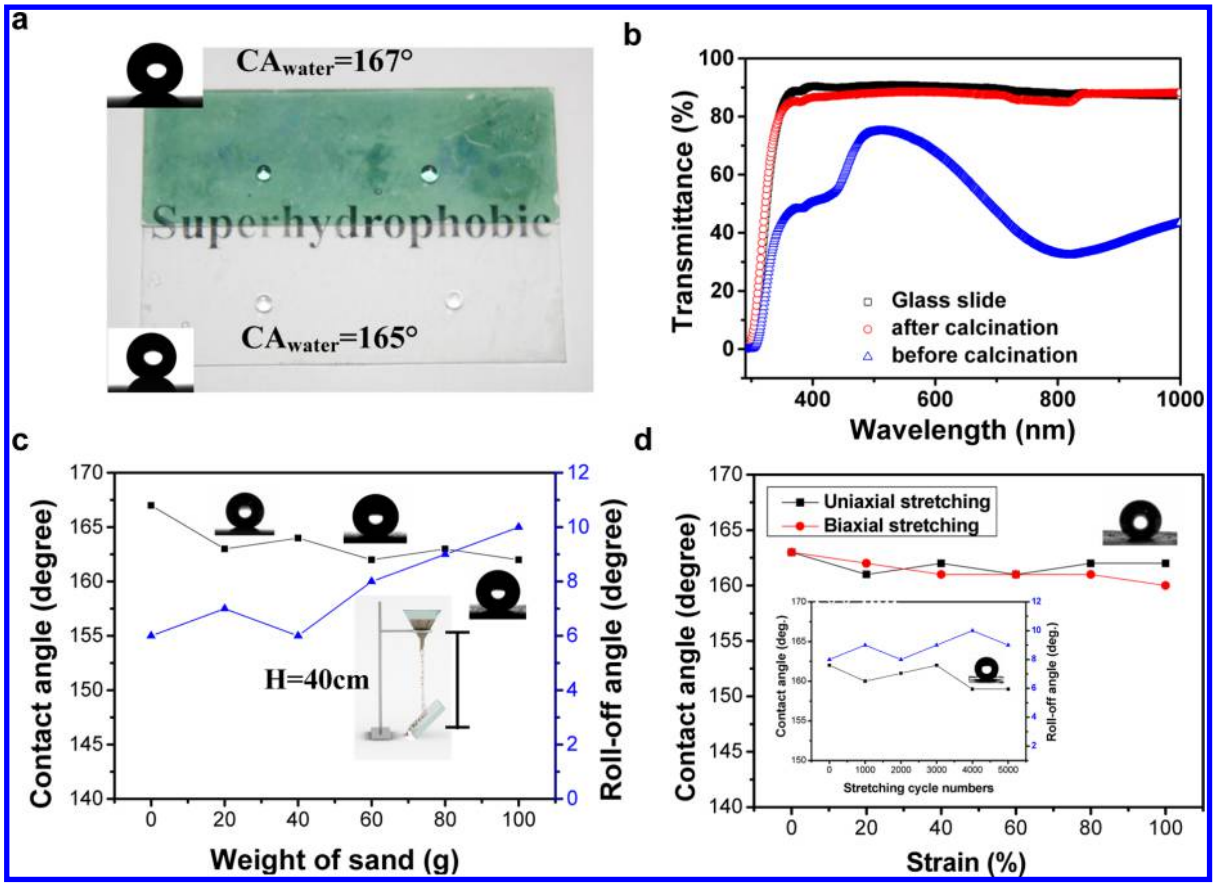

Figure 2. Optical and mechanical properties of the superhydrophobic coatings. (a) Digital photographs of the superhydrophobic silica/PAni hybrid (upper part) and silica coating (lower part). (b) Ultraviolet−visible transmittance spectra of silica/PAni coating and silica-only coating as compared to pristine glass substrate. (c) The CAs and TAs on the silica/PAni coating after impinging tests with different weights of sand (inset, schematic of sand impinging experiment H = 40 cm). (d) The measured CAs on the uniaxially and biaxially stretched hybrid coating at different strains, respectively (inset, CAs and TAs on the uniaxially stretched coatings).

wall thickness of the silica nanotubes is approximately 10 nm as shown as the TEM image in the inset of Figure 1f.

The silanized coatings exhibit excellent superhydrophobic properties and can be realized on virtually any substrates (Table 1) because the hydrogel precursor solution has good wettability on different substrates and even good infiltrability in porous substances. Figure 1b shows a large superhydrophobic filter paper with a diameter of 18 cm exhibiting static CA of approximately 157° (note that 5 μL was the standard volume of water droplet for all surface property measurement in this study). The CAs on the hybrid silica/polymer coated wood and cotton fabric substrates were 160 and 165°, respectively (Figure 1c). The hybrid coating on cement exhibited CA as large as 174°. Water drops on coated glass substrate showed low hysteresis between advanced and receding angles as ∼6° (see Supporting Information S2 for more details). The TA of coatings on glass and cement substrates were as low as 6 and 7°, respectively, indicating the potential self-cleaning effect. The CAs were found to be almost independent with the thicknesses of the coatings (varied from 750 nm to 65 μm), which is likely due to the homogeneous microstructure of the coating. Note that the wetting and infiltrability of precursor solution is crucial for water-proof coatings on porous substrates, which enhance the durability and antiscrubbing ability by forming superhydrophobic structures into the deeper texture of substrates. Moreover, the in situ solution based gelling processes are readily compatible with scalable coating techniques such as dip coating, spray coating,[19] and inkjet printing,[16] and are also capable of producing superhydrophobic coatings on highly curved surfaces. We fabricated uniform superhydrophobic coating on a 10 cm × 10 cm glass substrate by a simple dip coating process.

The hydrogel based surfaces can be used to make transparent, superhydrophobic thin films, which are desirable for applications such as antifog and self-cleaning goggles and windshields.[20−22] Figure 2a presents transparent superhydrophobic surfaces based on the silica/PAni hybrid (the green and upper one) and the silica-nanotube only coating (the colorless and lower one) on glass substrates. The 2 μm-thick silica/PAni coated glass yielded a CA of 167° and a TA of 6°. Colorless coatings can be produced by removing the PAni component by either calcinating at 400 °C for 2 h or reacting with concentrate nitric acid at room temperature for 10 min, which is composed of solely silica nanotubes on glass (Figure 2a) or poly(dimethylsiloxane) (PDMS) substrate. The colorless coating on elastic PDMS shows CA of 165° and TA angle of 5°. The transmittance of the coating is reduced by less than ∼2% as compared to that of pristine glass in the full range of ultraviolet−visible spectrum measured (Figure 2b) (here the transmittance was defined as the integral area of the curve of the silica coated glass divided by that of a bare glass).

The antiabrasive property of as-fabricated superhydrophobic surfaces was further evaluated. The antiabrasion test was performed on a 2 μm-thick hybrid coating on glass by

dx.doi.org/10.1021/nl5019782 | Nano Lett. 2014, 14, 4803−4809

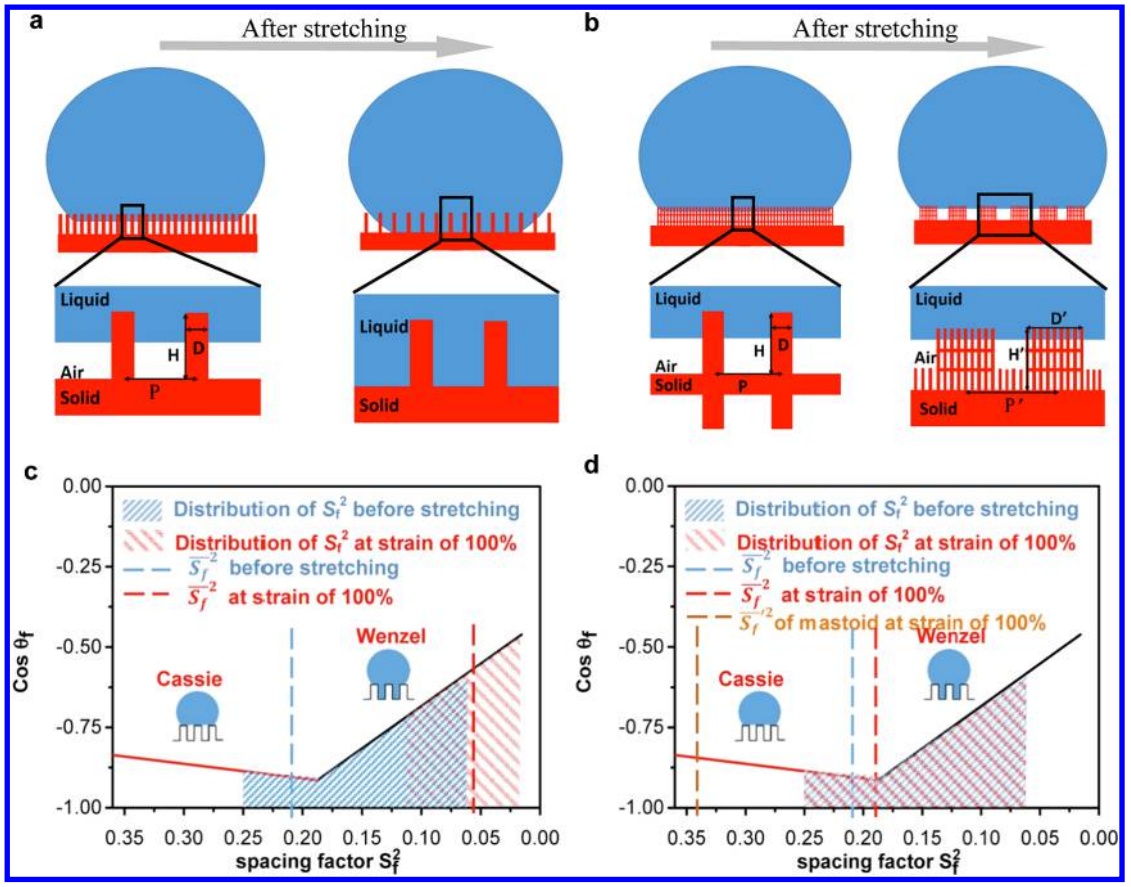

Figure 3. Effects of the geometric parameter, spacing factor S_f, on the Wenzel–Cassie transition in different conditions: (a,c) on 2D nanopillar array; (b,d) on 3D multiscale nanofiber networks. (a) Schematic of stretching a 2D nanopillar array, showing the surface undergoes a transition of the Cassie–Baxter state and Wenzel state. (b) Schematic of stretching a hierarchical hybrid coating, where strain-induced formation of multiscale structure resulted in stable Cassie state and kept the surface superhydrophobic under large strains. (c) Plot of cos θ_f as a function of the spacing factor S_f^2 for 2D nanopillars. $\overline{S_f}$ denotes the average value of S_f. The shading corresponds to the range of nanopillar array before (blue) and at strain of 100% (red). At 100% strain, the $\overline{S_f}$ value exceeds the Cassie–Wenzel transition point and the film loses superhydrophobic property. (d) Plot of cos θ_f as a function of S_f for 3D multiscale nanofiber networks. S_f corresponds to the spacing factor of nanofibers and S_f' corresponds to that of mastoids. Blue shading corresponds to the coating before stretching, while red one corresponds to after stretching at strain of 100%. Yellow dash denotes the measured $\overline{S_f}'$ corresponding to geometric parameters of mastoids at 100% strain. The formation of multiscale mastoids domains resulted in stable Cassie state of the surface.

impinging sand grains of 100–300 μm in radius to the surface from a height of ~40 cm (inset of Figure 2c), which corresponds to an impinging energy of 3.3×10^{-8} to 89×10^{-8} J per grain. The CAs and TAs of the coating were measured after every 20 g sands impinging (Figure 2c). The hybrid coating could sustain its superhydrophobic property up to 100 g of sands abrasion, superior to other thin films consisting of stacked particles. For example, silica-coated polystyrene spheres can only sustain superhydrophobic property with the same size impinging-sand from height up to 30 cm (impinging energy ~2.4×10^{-8} J per grain).[23] The antisand-abrasion property of the hybrid coating should be attributed to the unique interconnected network structure of silica/polymer composite nanofibers. The integrity of self-similar 3D microstructures of the coating enabled its superhydrophobicity to be well maintained before the coating was worn out. Moreover, the coating showed robust mechanical strength and good adhesion to substrates that it can sustain under peeling with scotch tape and still retain its superhydrophobic property afterward.

The hydrogel-based surfaces exhibited the capability to maintain its superhydrophobicity even when it was stretched with large strains. In a typical stretching test, the hybrid coating was first applied on PDMS substrates, the static CAs were then measured when the substrates were uniaxially and biaxially stretched to different strains. The coating can keep the CA ~ 160° and TA less than 10° under biaxial strains in the range of 0–100% and has no noticeable decay of its superhydrophobic property under uniaxial strain of 100% cycled 5000 times, as shown in Figure 2d. Moreover, a slight anisotropism of surface property could be induced to the thin film by simply stretching the coating and the TAs exhibited to be of ~2° difference in the directions parallel and perpendicular to stretching (see Supporting Information S2 for more details). In addition, the superhydrophobicity of the coating showed excellent stability and uniformity that the water drop kept almost the same large CA when the water droplet was moved in an area of several centimeters on the coating that has been statically stretched to 100% strain. The superhydrophobic property of our stretchable coating is superb as compared to any other reported flexible superhydrophobic coatings. For example, the PDMS modified by mechanically assembled monolayers has the highest water CA ~131° while being stretched to different strains.[24] PDMS with molded 2D nanopillar array keep CA of 156° at the

dx.doi.org/10.1021/nl5019782 | Nano Lett. 2014, 14, 4803–4809

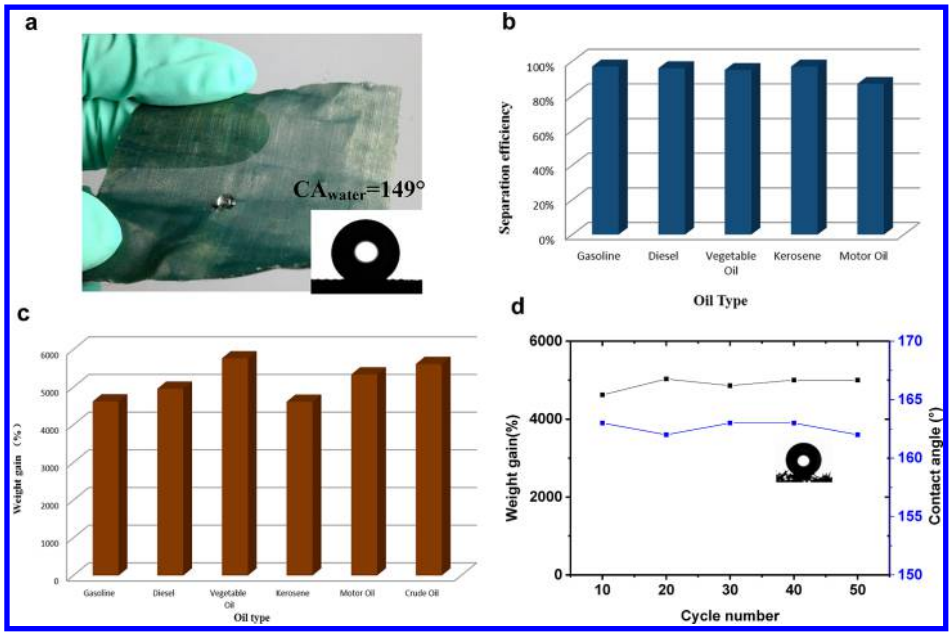

Figure 4. Oil/water separation by the silica/PAni-coated screen (a,b) and oil–selective absorption of the silica/PAni-coated sponge (c,d). (a) The deposition of a water drop on the coated screen was similar to that on a lotus leaf. (b) Oil/water separation efficiency of the silica-PAni-coated screen filter. (c) Absorption capacities of the silica/PAni-coated sponge for various oils. (d) Cycling experiment for gasoline absorption using the superhydrophobic sponge. Inset, CAs of the sponge after 50 cycles of squeezing.

highest 30% strain.[25] McKinley et al. observed that the Cassie–Wenzel transition and oleophobic/oleophyllic transition at 30% strain on fluorodecyl polyhedral oligomeric silsesquioxane-coated fabric surfaces.[26] Such kind of flexible, stretchable, and superhydrophobic coating will have important applications in the field of electronic skin and wearable devices.[27]

To understand the robust superhydrophobic property of the stretchable coating, we investigated its morphology change at different strains by SEM characterization. The stretched coating was chapped to form mastoid domains with diameters of approximately 3–5 μm. The formation of the mastoid domains in the coating was likely attributed to the yield-induced neck formation within the coating layer under large strains. Magnified SEM image showed that the morphology and size of nanofibers inside the mastoid domains remained unaltered as those in the unstretched film (see Supporting Information S3 for details).

The formation of mastoid domains endows the coating stable and robust superhydrophobic properties against strains. We analyzed the relationship between the surface property and endured strain of our coating and made a comparison with that of a hydrophobic 2D nanofibers array. Note the 2D micro/nanofibers array is one of the most widely used morphology and simulation model for superhydrophobic layers.[7] It should be mentioned that the Cassie–Baxter relation is determined by thermodynamic equations for the free surface energies, and some authors proposed that wetting can be dominated by contact line pinning.[28,29] Our analysis was based on the assumption that Cassie–Baxter relation is valid within the subject investigated. It is well-known that superhydrophobic property, that is, the Cassie state, depends on surface geometric parameters to keep microscopic pockets of air and dewet the liquid droplet. For patterned hydrophobic surface, a dimensionless spacing factor $S_f = D/P$ is the critical parameter for determining the transition between Wenzel and Cassie states[30,31] (where D is the diameter of bumps and P is the pitch distance between them). Mechanical deformation such as stretching could lead to the changes of the spacing factor,[26] and hence result in a completely wetted Wenzel state[32] when the spacing factor reaches a Cassie–Wenzel transition point. In the case of superhydrophobic 2D nanofiber array (in Cassie state), stretching leads to a steeply decreased value of S_f^2 to $S_{f\,\mathrm{stretched}}^2 = S_{f\,\mathrm{unstretched}}^2 (1/(1+\varepsilon)^2)$. (Figure 3a, ε is the mechanical strain), such that the pitch distance P increases for a fixed value of the bump diameter D. On the basis of the Cassie–Baxter relation, the apparent contact angles on the stretched fabric can then be estimated as

$$\cos\theta_{c\,\mathrm{stretched}} = \frac{\pi}{4} S_{f\,\mathrm{stretched}}^2 (1+\cos\theta_{\mathrm{flat}}) - 1 = -1 + \left(\frac{1}{1+\varepsilon}\right)^2 (1+\cos\theta_{c\,\mathrm{unstretched}}) \quad (1)$$

Therefore, the film will transition into a Wenzel state and lose its superhydrophobicity when the S_f^2 value is smaller than the Wenzel/Cassie transition point (Figure 3a). However, our 3D hierarchical nanostructured coating can maintain the superhydrophobic state under large strains (Figure 3b), based on two main factors: First, the mastoid domains (with diameter D' and pitch distance P') were nonwettable by water because the S_f^2 of the nanofibers inside the mastoids was still kept in the range of Cassie state (note that the nanofibers inside the mastoid domains had the similar morphology and size as those in the unstretched film). Second, the value of $S_f'^2$ of the micron-sized mastoid domains was calculated to be ~0.34 according to the parameters of the coating stretched at 100% biaxial strain, which is much larger than that of the Wenzel/Cassie transition point (Figure 3d). Therefore, such a multigeometric-scaling structure effectively increased the stability of the Cassie state (i.e., superhydrophobic state) while the coating was stretched. (See Supporting Information S3 for detailed discussion.) This unique multigeometric-scaling mechanism of hierarchical micro/nanostructures is expected to be useful for designing

dx.doi.org/10.1021/nl5019782 | Nano Lett. 2014, 14, 4803–4809

the long-live stretchable/bendable superhydrophobic coatings under large strains in future.

For applications in environmental preservation such as oil spill cleanup and oil recovery from industrial oily wastewater, high-efficiency oil/water separation materials are critically needed. We developed an oil/water filter by applying the hybrid coating on a 200 mesh stainless steel screen (Figure 4a,b), which selectively separate oils from water. The coated screen exhibited surface properties exactly like a lotus leaf with an apparent CA of 149° and water droplet beading up and rolling off the hydrophobic screen easily (Movie S1, Supporting Information). A screen tube was used to enable the continuously separation of oil/water mixture. The filter was both superhydrophobic and superoleophilic, such that the oils, but not the water, transfluxed through the modified screen. Various types of oils including gasoline, diesel, vegetable oil, kerosene, and motor oil were successfully separated from water in the mixtures with separation efficiency exceeding 90% (Figure 4b) and the residue water contents in the separated oils were measured to be less than 0.04% (see Supporting Information S4 for more details), which is comparable to other selective filters such as self-assembled monolayer treated nickel foam,[33] PVDF microstructured membrane,[34] and fluorodecyl POSS+x-PEGDA blend coated stainless-steel mesh.[35] However, our hybrid coatings show the advantages of low fabrication cost and the potential for industry scale fabrication, showing great promise as large-area selective filters for industry oil recovery and oil spill handling.

The hybrid coating was also investigated as an oil−selective absorption material. By applying a commercial available sponge with the hybrid coating, we produced a superhydrophobic and superoleophilic oil absorber that may work in harsh environments. The selective collection of crude oil from seawater was performed by placing the superhydrophobic sponge in a 40 g·L^{-1} aqueous solution of sea salt with a crude oil layer with 100 rpm oscillation shaking to simulate a crude oil spill in the natural environment. As shown in Figure 4c, the sponge reliably absorbed up to 40× its weight of different oils. The absorbed oils can be recollected by simple squeezing the sponges. Given the robust and flexible hybrid coating, the sponge exhibited a long cycle life that it retained superhydrophobicity and high-absorption capability even after 50 cycles of absorbing and squeezing (Figure 4d). Compared with other oil absorption materials, for example, graphene sponges,[36] MnO_2 nanowire membrane,[4] silicone nanofilament-coated polyester textiles,[37] carbon nanotube sponges,[38] and polydivinylbenzene,[39] our oil absorption sponges based on the hybrid coating have potential advantages as follows: facile processing, industrial scale production potential, low cost, high-absorption capacity, excellent cyclability, long life, and adaptable for harsh ambient environments.

In summary, we demonstrate here a novel two-step design to utilize the inherent 3D hierarchical nanostructure of hydrogel matrix as a template to produce transparent, durable superhydrophobic surfaces with multiple functionalities. This hydrogel-based templating method offers a general yet versatile approach to land the stable superhydrophobicity onto virtually any surfaces, via a highly scalable process such as dip coating or spray coating techniques. Our superhydrophobic surfaces exhibit excellent mechanical properties in terms of robustness and stretchability. We envision that the hydrogel templated superhydrophobic surfaces will find practical applications in low-cost, robust, transparent and long-life water-proof coatings, antifouling surfaces, and selective absorption materials for environmental preservations.

■ ASSOCIATED CONTENT

Ⓢ Supporting Information

Experimental details, further measurement of surface properties, analysis, and additional SEM characterizations. This material is available free of charge via the Internet at http://pubs.acs.org.

■ AUTHOR INFORMATION

Corresponding Authors

*E-mail: (L.P.) ljpan@nju.edu.cn.
*E-mail: (Y.S.) yshi@nju.edu.cn.
*E-mail: (G.Y.) ghyu@austin.utexas.edu.

Author Contributions

‖Y.W. and Y.S. contributed equally to this work.

Notes

The authors declare no competing financial interest.

■ ACKNOWLEDGMENTS

G.Y. acknowledges the financial support of faculty start-up grant from the University of Texas at Austin and Ralph E. Powe Jr. Faculty Award. L.P. and Y.S. are thankful for funding support from the Chinese National Key Fundamental Research Project (2013CB932900, 2011CB92210), the National Natural Science Foundation of China (61229401, 61076017, and 60990314), the Programs of NCET and the PAPD.

■ REFERENCES

(1) Cassie, A. B. D.; Baxter, S. *Trans. Faraday Soc.* **1944**, *40*, 0546−0550.
(2) Liu, K. S.; Yao, X.; Jiang, L. *Chem. Soc. Rev.* **2010**, *39*, 3240−3255.
(3) Deng, X.; Mammen, L.; Butt, H. J.; Vollmer, D. *Science* **2012**, *335*, 67−70.
(4) Yuan, J. K.; Liu, X.; Akbulut, O.; Hu, J.; Suib, S. L.; Kong, J.; Stellacci, F. *Nat. Nanotechnol.* **2008**, *3*, 332−336.
(5) Wong, T. S.; Kang, S. H.; Tang, S. K. Y.; Smythe, E. J.; Hatton, B. D.; Grinthal, A.; Aizenberg, J. *Nature* **2011**, *477*, 443−447.
(6) Feng, L.; Li, S. H.; Li, Y. S.; Li, H. J.; Zhang, L. J.; Zhai, J.; Song, Y. L.; Liu, B. Q.; Jiang, L.; Zhu, D. B. *Adv. Mater.* **2002**, *14*, 1857−1860.
(7) Kumar, R. T. R.; Mogensen, K. B.; Boggild, P. *J. Phys. Chem. C* **2010**, *114*, 2936−2940.
(8) Cao, L.; Price, T. P.; Weiss, M.; Gao, D. *Langmuir* **2008**, *24*, 1640−1643.
(9) Rouessac, V.; Ungureanu, A.; Bangarda, S.; Deratani, A.; Lo, C. H.; Wei, T. C.; Lee, K. R.; Lai, J. Y. *Chem. Vap. Deposition* **2011**, *17*, 198−203.
(10) Xu, L. G.; He, J. H. *Langmuir* **2012**, *28*, 7512−7518.
(11) Kim, S. H.; Lee, S. Y.; Yang, S. M. *Angew. Chem., Int. Ed.* **2010**, *49*, 2535−2538.
(12) Karunakaran, R. G.; Lu, C. H.; Zhang, Z.; Yang, S. *Langmuir* **2011**, *27*, 4594−4602.
(13) Erbil, H. Y.; Demirel, A. L.; Avci, Y.; Mert, O. *Science* **2003**, *299*, 1377−1380.
(14) Tuteja, A.; Choi, W.; Ma, M.; Mabry, J. M.; Mazzella, S. A.; Rutledge, G. C.; McKinley, G. H.; Cohen, R. E. *Science* **2007**, *318*, 1618−1622.
(15) Tuteja, A.; Choi, W.; Mabry, J. M.; McKinley, G. H.; Cohen, R. E. *Proc. Natl. Acad. Sci. U.S.A.* **2008**, *105*, 18200−18205.
(16) Pan, L. J.; Yu, G. H.; Zhai, D. Y.; Lee, H. R.; Zhao, W. T.; Liu, N.; Wang, H. L.; Tee, B. C. K.; Shi, Y.; Cui, Y.; Bao, Z. *Proc. Natl. Acad. Sci. U.S.A.* **2012**, *109*, 9287−9292.

(17) Stöber, W.; Fink, A.; Bohn, E. *J. Colloid Interface Sci.* **1968**, *26*, 62−69.
(18) Nosonovsky, M. *Langmuir* **2007**, *23*, 9919−9920.
(19) Hecht, D. S.; Hu, L.; Irvin, G. *Adv. Mater.* **2011**, *23*, 1482−1513.
(20) Liu, Y. Y.; Chen, X. Q.; Xin, J. H. *Nanotechnology* **2006**, *17*, 3259−3263.
(21) Han, J. T.; Kim, S. Y.; Woo, J. S.; Lee, G. W. *Adv. Mater.* **2008**, *20*, 3724−3727.
(22) Chiou, N. R.; Lui, C. M.; Guan, J. J.; Lee, L. J.; Epstein, A. J. *Nat. Nanotechnol.* **2007**, *2*, 354−357.
(23) Deng, X.; Mammen, L.; Zhao, Y.; Lellig, P.; Muellen, K.; Li, C.; Butt, H. J.; Vollmer, D. *Adv. Mater.* **2011**, *23*, 2962−2965.
(24) Genzer, J.; Efimenko, K. *Science* **2000**, *290*, 2130−2133.
(25) Lee, S. G.; Lee, D. Y.; Lim, H. S.; Lee, D. H.; Lee, S.; Cho, K. *Adv. Mater.* **2010**, *22*, 5013−5017.
(26) Choi, W.; Tuteja, A.; Chhatre, S.; Mabry, J. M.; Cohen, R. E.; Mckinley, G. H. *Adv. Mater.* **2009**, *21*, 2190−2195.
(27) Hammock, M. L.; Chortos, A.; Tee, B. C. K.; Tok, J. B. H.; Bao, Z. *Adv. Mater.* **2013**, *25*, 5997−6037.
(28) Gao, L.; McCarthy, T. J. *Langmuir* **2007**, *23*, 3762−3765.
(29) Papadopoulos, P.; Mammen, L.; Deng, X.; Vollmer, D.; Butt, H. J. *Proc. Natl. Acad. Sci. U.S.A.* **2013**, *110*, 3254−3258.
(30) Bhushan, B.; Nosonovsky, M.; Jung, Y. C. *J. R. Soc. Interface* **2007**, *4*, 643−648.
(31) Nosonovsky, M.; Bhushan, B. *Nano Lett.* **2007**, *7*, 2633−2637.
(32) Wenzel, R. N. *Ind. Eng. Chem.* **1936**, *28*, 988−994.
(33) Cheng, M.; Gao, Y.; Guo, X.; Shi, Z.; Chen, J. F.; Shi, F. *Langmuir* **2011**, *27*, 7371−7375.
(34) Zhang, W.; Shi, Z.; Zhang, F.; Liu, X.; Jin, J.; Jiang, L. *Adv. Mater.* **2013**, *25*, 2071−2076.
(35) Kota, A. K.; Kwon, G.; Choi, W.; Mabry, J. M.; Tuteja, A. *Nat. Commun.* **2012**, *3*, 1025.
(36) Niu, Z.; Chen, J.; Hng, H. H.; Ma, J.; Chen, X. *Adv. Mater.* **2012**, *24*, 4144−4150.
(37) Zhang, J. P.; Seeger, S. *Adv. Funct. Mater.* **2011**, *21*, 4699−4704.
(38) Gui, X.; Wei, J.; Wang, K.; Cao, A.; Zhu, H.; Jia, Y.; Shu, Q.; Wu, D. *Adv. Mater.* **2010**, *22*, 617−621.
(39) Zhang, Y.; Wei, S.; Liu, F.; Du, Y.; Liu, S.; Ji, Y.; Yokoi, T.; Tatsumi, T.; Xiao, F. S. *Nano Today* **2009**, *4*, 135−142.

dx.doi.org/10.1021/nl5019782 | *Nano Lett.* 2014, 14, 4803−4809